

Tracking ring rolling geometry using cameras

Matthew R. Arthington*, Christopher Cleaver†, Julian Allwood‡, Stephen Duncan§

*§Department of Engineering Science
Parks Road
Oxford, OX1 3PJ, UK

†‡Department of Engineering
University of Cambridge
Trumpington Street
Cambridge, CB2 1PZ, UK

matthew.arthington@eng.ox.ac.uk*, cjc82@cam.ac.uk†, jma42@cam.ac.uk‡, stephen.duncan@eng.ox.ac.uk§

Abstract—Ring-rolling is an industrial forming process to produce high-strength metal rings up to 6m diameter. Thick-walled cylindrical workpieces of material, typically metallic alloys, are compressed between two or more internal and external rollers and rotated until a target geometry, often outer diameter, is achieved. The process is inherently unstable and the process is often constrained and/or controlled to improve its stability. This paper presents an image processing algorithm for the measurement of ring geometry through photogrammetry in real-time. These measurements will form part of the feedback control system for a ring-rolling process. An off-the-shelf USB webcam is used to capture images of the ring during forming and the scene is controlled to maximise contrast and minimise occlusions of the ring. The image processing tasks include object identification, edge detection, outlier rejection and distortion rectification. The process has been implemented on a desktop-scale forming machine and has been shown to work at rates suitable for control the ring-rolling process using feedback.

I. INTRODUCTION

Ring-rolling is an industrial metal forming process for producing high-strength rings up to 6m in diameter. Industry data puts 2011 ring worldwide hot ring rolling production at 1.7 million tonnes, some 6% of the total forging market [1]. Typical applications include ring components for aerospace engines, energy turbines (including Industrial Gas Turbines and Steam Turbines), pipe fittings for oil and gas and petrochemical industrials and various engineering components in shipping, mining, construction and other industries [1]. In addition to hot ring rolling, cold ring rolling is used to produce smaller ring products such as automotive bearings. As a forging process, it produces a higher strength ring than alternative casting techniques, whilst it can be quicker and less materially wasteful than alternative forging methods [2]. In the ring rolling process, a thick walled cylindrical workpiece is transformed into a thinner walled, large diameter ring [3]–[5] by compressing the wall between rotating rollers see figure 1. Ring-rolling is usually significantly faster than open-die or closed-die forging and this is the key reason it is used widely in industry.

Manual feedback has been used for many years to control the amount of ‘roll-gap’, the distance between the radial forming rollers, as has open-loop control. Recently, feedback

control has been employed to automatically achieve the desired ring outer diameter.

In order for feedback control to work efficiently in ring rolling, sensors need to measure geometry with sufficient accuracy and frequency. However, the process - with only one driven roll acting on the outer diameter - is inherently unstable and leads to significant ring oscillations about the roll gap as indicated in figure 2, even with the addition of stabilising guide rolls [6]. Single-point sensors, such as contacting rollers and optical distance sensing devices, provide scalar geometry measurements with high accuracy and at a high frequency, but do not capture overall geometry, a particular problem if the ring workpiece is transiently off-centre. Multiple measurements may be made, but this increases the cost of the measurement hardware. In industrial practice, large forging tolerances are added to the target geometry partially to allow for such inaccuracies [2]. In order to increase the geometry information provided by sensing, the development of image processing algorithms to detect ring geometry has begun [7], [8].

An image processing system has the advantages of measuring multiple points around the ring simultaneously and lower cost, with the disadvantage of reduced accuracy and measurement frequency when compared to a laser distance measurement. Meier et al. [8] have made early attempts at implementing an image processing system using proprietary hardware systems to move a state-of-the-art measurement camera with a ring as it deforms. This effort was implemented on industrial scale ring-rolling machinery, which proved that the high temperatures encountered during the process were not a significant barrier. The work of Meier et al. did not describe their image processing algorithm in detail, and that effort continues.

This paper presents a new image processing algorithm which allows the real-time measurement of the ring-rolling process using ‘cheap’ hardware. The algorithm permits the estimation of high-density radius data for the ring’s inner and outer edge. The methods for overcoming problems with lens distortion, imperfect camera alignment, difficult lighting and false edge points are described.

The measurement system has been implemented on a

desktop scale ring-rolling machine using Plasticine® as its working material. Plasticine® as a strain and strain rate hardening clay that exhibits yield has been widely used to models the behaviour of hot metalworking processes; indicating likely deformation behaviour and force estimates [9]–[12]. This machine is novel with respect to the flexibility of its configuration [13], [14], and the primary objective of this work is to develop a system that can be used as the sensor in the feedback control of the flexible ring-rolling process.

The novel contribution of this work is that of the prescient use of fast procedures to find and identify the geometry of the ring accurately, leading to real time ring measurement. It is not the intention of this paper to go into great depth in describing each of the image processing operations, which are described completely in texts such as [15], [16]. The novel contribution of this work is that of the prescient use of ‘fast’ procedures to find and identify the geometry of the ring accurately.

The paper is laid out as follows: Section II describes the hardware, image acquisition and inputs required for the process. Section III describes how these are used to automatically measure the ring geometry using image processing techniques. Section IV gives an example of the data that may be obtained from the system in a ring being processed by the desktop ring-rolling machine. Section V concludes the paper.

II. IMAGING

The flexible ring-rolling machine has many possible configurations with regards to the shape, size and number of radial and axial rollers. The process focused on here was that of two support rollers under the ring and two forming tool pairs: radial compression rollers and axial compression rollers. This is a configuration often found in industry [4], [5], however there are usually additional ‘guide rollers’ in industrial processes, which prevent extraneous movement of the ring due to the aforementioned instability. By sensing the position of the ring and controlling the speeds of the forming motors the ring can be stabilised without mechanical constraints. The machine configuration is shown in figure 1.

The ring was photographed by a USB web camera - in this case a Logitech HD Pro Webcam C920 - with its optical centre placed on the initial axis of the ring and its image plane perpendicular to that axis. This was done manually, and any image misalignment was corrected by software, as described in section II. The PC used for the process was a 64-bit Intel i7 4770 CPU running at 3.4GHz, with 16GB of RAM running Microsoft Windows 7. The software was written in MATLAB® 2013a. Surfaces seen behind the ring in the image were covered with a diffuse black material to achieve a large contrast against the white Plasticine®. The scene was lit using ambient light. Significant occlusions of the ring arose because of the two forming tools, which could not be removed; they are evident in figure 2. These tools move radially outwards as the ring grows to accommodate its growing diameter. Other undesirable imaging artefacts arise from the specular reflections from the supporting rollers.

To assist the image processing and calibration process, certain manual inputs are given to the software. These include: a rectangular region of interest within which the ring is expected to remain throughout the forming process; estimates

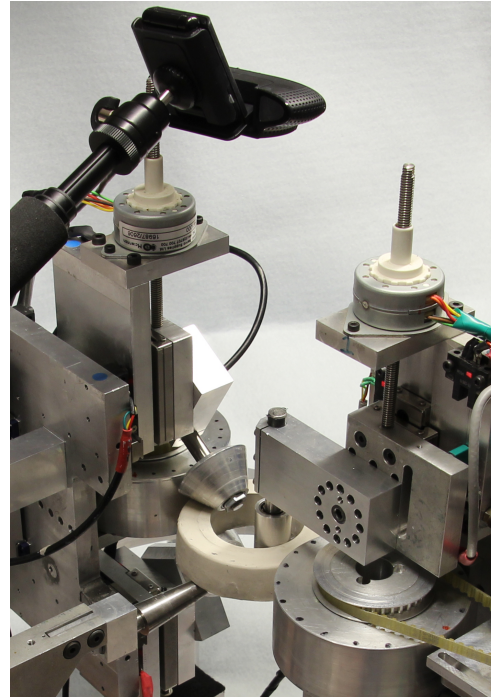


Fig. 1. The Plasticine® ring rolling machine showing the white Plasticine® ring. The supporting rollers hold the weight of the ring. The conic axial forming rollers and the radial forming rollers are all in contact with the ring.

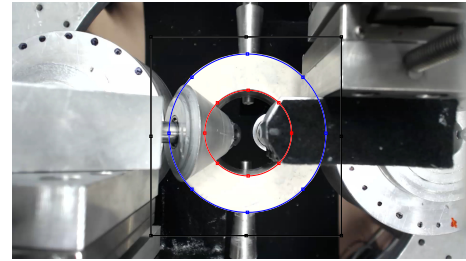


Fig. 2. The image captured by the webcam overlaid with the manually chosen regions of interest. The ring typically oscillates vertically with some rotation about the right hand radial roll gap when the angular velocities of the rollers are equal.

of the initial elliptical inner and outer edges of the ring; polygonal regions covering the forming tools and the likely positions of specular reflections.

Other inputs to the process before the forming begins are the camera calibration parameters. These include the intrinsic parameters, those inherent to the camera, and the transformation matrix that relates the camera image plane to the plane of the ring’s upper surface. These were estimated using two procedures, the first was imaging a checker-board grid of black and white squares of known dimension at several orientations to find the camera’s optical centre, radial distortion parameters, etc. This task was performed using the Camera Calibration Toolbox for MATLAB® [17]. The second, estimating the ring plane with respect to the camera, was performed by placing a pattern of concentric circles onto the ring and photographing it before the forming began. Once the rectification of the intrinsic distortion was corrected, the edges of this pattern of rings were found and their elliptical shape estimated to calculate

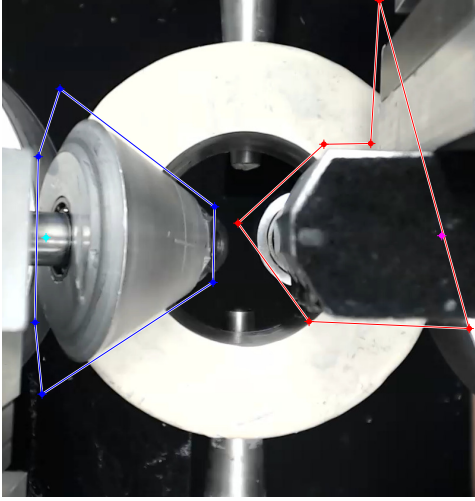


Fig. 3. The cropped image with tool regions manually identified. The turquoise and magenta points control the translation of these tool regions as the outer edge grows in diameter. In this example the cropped image has a resolution of 611×643 .

the perspective transformation required to observe the ring in its top plane. The interested reader may find out more about these homography transformations from [16].

Throughout the forming process, images are captured and processed sequentially. Image capturing and processing were performed in parallel. The processing of each frame relies on data from the previous frame and takes significantly longer than the image capture step. The processing time is therefore the critical factor in improving the measurement frequency.

III. IMAGE PROCESSING

The purpose of the image processing algorithm is to produce a reliable, accurate, estimate of the ring geometry as quickly as possible. A compromise between the accuracy and the speed requirement had to be made in several instances, with the constraints on required performance dictating that compromise.

The image processing tasks are summarised in figure 4.

A. Capture image

The image is captured and the data stored as a size $N \times M \times 3$ intensity RGB matrix. This matrix is made into an $N \times M \times 1$ greyscale image by taking the average intensity of the three colour channels. The resolution used during these experiments was the maximum of 1920×1080 , which permitted the greatest accuracy. The increase in transfer speed when using a lower resolution was not significant enough to justify a lower accuracy.

B. Crop image

An elliptical-fit to the points of the outer edge of the ring from the previous frame were used to estimate the centre and maximum radius of the current frame. This centre and maximum radius, plus a small constant to allow for growth and translation, were used to estimate the limits of the ring's horizontal and vertical movement. The image was cropped

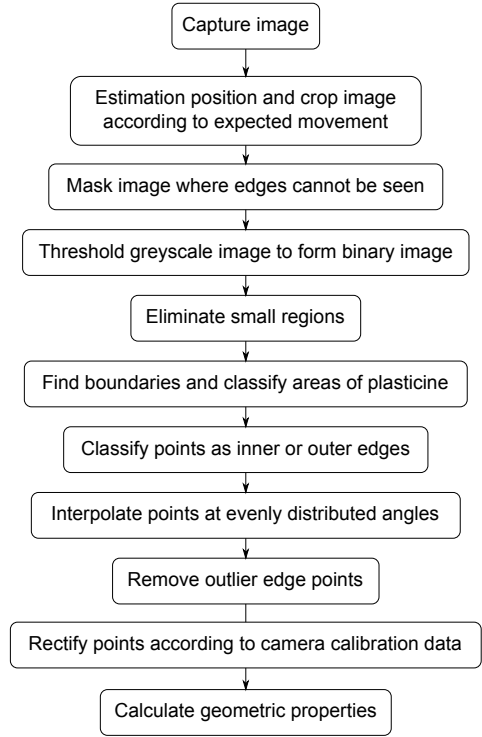


Fig. 4. The image processing algorithm.



Fig. 5. The masked image.

according to these limits to result in an $n \times m$ matrix. This is done to reduce the computation time of subsequent image-wide morphological operations.

C. Create binary mask

The positions of the tool regions and specular highlight regions are calculated based on the centre and radii from the previous frame. Each region is defined by a manually-drawn polygon and a base-point which is used to translate the polygon as the ring expands. The base-point is attached to a circle defined by the mean radius of the outer edge of the ring, the ring's original centre, and an angle with respect to that centre along which to move. Figure 3 shows the tool regions

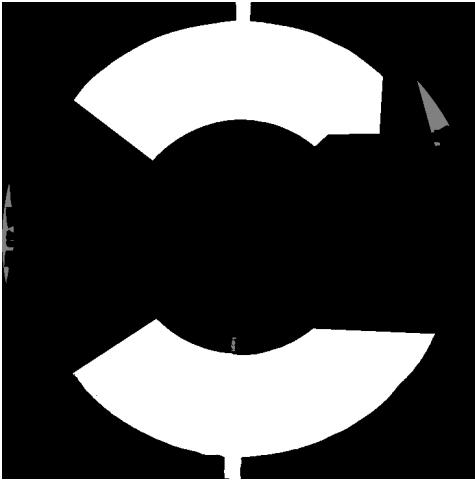


Fig. 6. The binary image, after thresholding the masked image, is shown in non-zero pixels. The small contiguous regions that were removed are shown in grey.

with their base points and figure 5 shows the resultant masked image.

Edge points are assumed not to have moved more than a constant distance from their previous location. To create a mask based on this assumption, the previous centre and the inner and outer radii, minus and plus a constant, consecutively, are used to create an annulus mask region. The annulus mask and the polygonal regions are combined to produce a single binary mask, which removes all areas in the image where edge points cannot be found. This is shown in figure 5.

D. Threshold image

The light coloured Plasticine® material of the ring contrasted with the dark background. In order to detect edges quickly, the high gradient between the light and dark regions was identified by setting all pixels with an intensity less than a constant value to zero and otherwise to 1. Although more sophisticated edge detection methods exist [18] that could find the edge of the ring to an accuracy of better (less) than 1 pixel, but the extra computation time required outweighed this benefit. The resulting binary image is shown in figure 6.

E. Eliminate small regions

The binary image was further processed to remove small contiguous regions of light or dark pixels. This was to eliminate the possibility of finding edge points at locations where noise in the image or slight variations in lighting conditions made the Plasticine® appear to contain holes or for Plasticine® to be apparent in the background. Figure 6 shows the holes that were removed in the example image.

F. Find bright boundaries and classify Plasticine®

The coordinates of the continuous boundaries of all bright regions were found. Not all bright regions that remained were Plasticine®, but the largest two regions were invariably the upper and lower halves of the ring. These were identified by selecting the two largest unconnected boundaries. The visible Plasticine® was then classified as the regions contained within

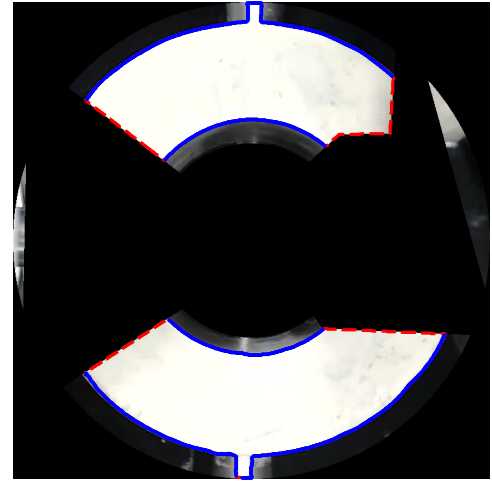


Fig. 7. The masked image showing the boundaries of the two brightest regions in blue. The dashed red line shows the boundaries that were rejected because they were too close to the mask.

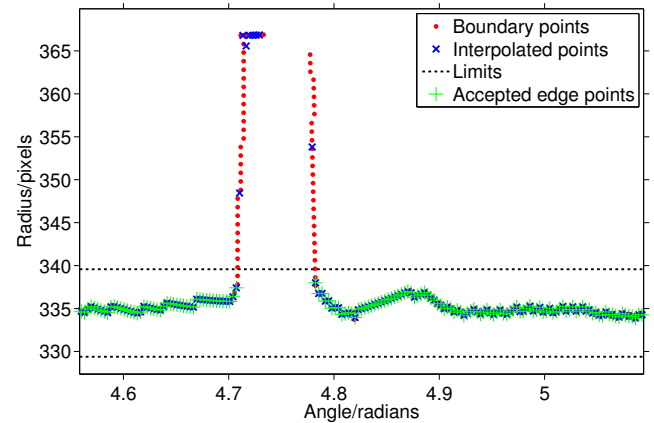


Fig. 8. A section of the region boundary plotted as radius against angle where a specular highlight has falsely been identified as Plasticine®. The interpolated points are sparse along the radial direction, but are dense where the boundary is circular. The limits, based on the interpolated mean and standard deviation, show the acceptable range of edge points.

these two boundaries. The positions of the inner and outer edges were initially identified as the boundary positions that were at more than 1.5 pixels from the binary mask. Figure 7 shows this boundary identification process.

G. Separate inner and outer edge points

The boundary points were then classified as belonging to the inner or outer edge of the ring based on their radius from the centre in the previous frame. Those that had a radius within a constant distance of the mean inner radius from the previous frame were classified as inner points, and similarly for outer points. Other points were rejected.

H. Interpolation of edge points

The shape of the ring is invariably circular and this was used to identify boundary points that are true ring-edge points. The radii of the points, calculated as their distance from the previous frame's centre, were linearly interpolated at evenly

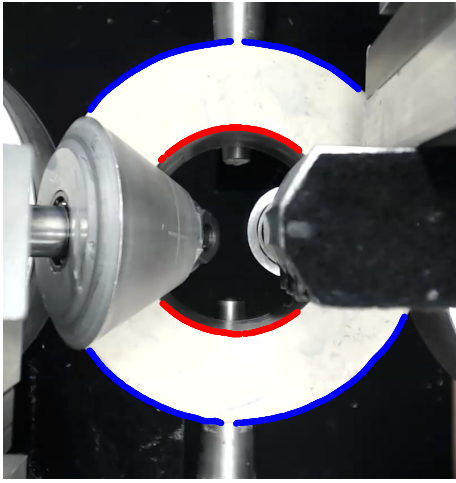


Fig. 9. The image with the points identified as true-edges of the ring.

distributed angles. The separation of the angles was calculated as the range of angles in the boundary points divided by their number. This interpolation had little effect on boundary points lying along a tangential arc, but radially aligned points would be reduced to a single point. The effect of this interpolation is shown in figure 8

I. Reject outlying edge points

Some boundary points would remain falsely identified as edge points. Further refinement of points was performed for the inner edge by rejecting points farther than 1 standard deviations from the median radius of the points that remain. The same process was applied to the outer points. This filtering process is suitable because the ring is expected to be approximately circular, and variations within the radii are expected to be closely bound to the median value. Figure 9 shows the edge points identified as true ring boundaries.

J. Point rectification

The edge points that remained were deemed to be true positions of the ring's inner and outer edges. These points were transformed into their real world positions by applying the rectification calculated before the forming started. Radial distortion was removed, and perspective transformation returned edge coordinates in mm.

K. Calculating geometric properties

The rectified two dimensional data could be used for a variety of different measurements of the ring geometry. The most important data from a control point of view was the vertical position of the ring's centre. The ring was not perfectly circular, and the asymmetry increased as it was formed, so an approximation was made that the ring edge points lay on an ellipse. This approximation is very good for all but the most distorted of shapes. Through the combination of many values to only 5 parameters, the elliptical fitting process reduces error from various sources, especially that from aliasing where edges are assumed to lie at the centre of the nearest pixel. The elliptical fit was used to estimate the position of the ring's centre, its major and minor axis lengths and the orientation

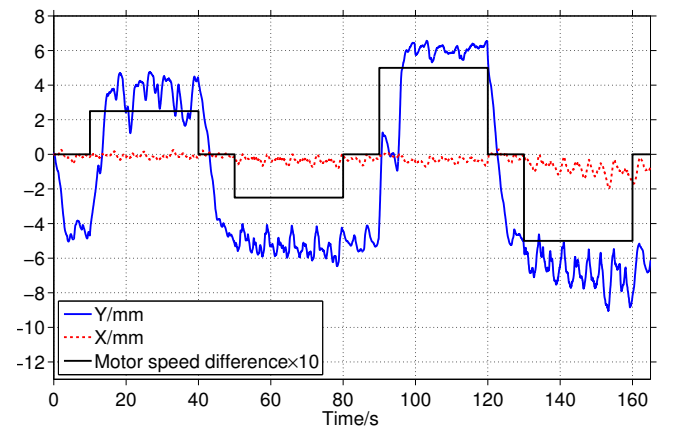


Fig. 10. Exemplary data from a run of the machine without forming. The Y displacement direction is the vertical direction in the images.

of these axes with respect to the machine. The centre position and radii were used as estimates for their values in next frame at each stage in the processing.

IV. RESULTS

This section presents the measurement data obtained from the image processing system from a recording of one experiment without forming. The data is important for the characterisation of the instability in the centre position of the ring, and would have been very difficult to obtain using single-point measurements. The frame rate of the recording was 30 fps (frames per second). If the data had been calculated in real-time the data density would have reduced to 2/3 of that seen here.

In this experiment all rollers were held at a fixed position, the radial roller had a constant angular velocity and the axial roller's angular velocity was different by a fraction of the radial velocity. Figure 10 plots some of the data obtained from that experiment. It can be seen that the ring centre moves away from the centred position even when the two roller speeds are equal. The control of this phenomenon was one of the primary motivations for this research.

The displacement of the centre in the X and Y directions can be seen to oscillate with a period of 7 s, the same as the rotation period of the ring. The oscillation was due to the asymmetry in the ring, which meant that the rings' centre position would orbit about a mean position. Measuring the geometry of the ring at a wide range of angles simultaneously allows the calculation of this asymmetry and permits the estimation of the true mean position for control of centring.

A. Accuracy

To estimate the error in calculating the centre position of the ring, a stationary ring was measured over 5 seconds at 30 fps. The standard deviation was 0.0016 mm with a ring diameter of 85 mm. The range of the Y measurement was 0.0090 mm. Without a more accurate measurement device it is difficult to estimate the absolute error in measuring ring geometry.

The sources of error when measuring the ring geometry are common to many photogrammetric systems. These include: uncontrollable changes in lighting conditions which make edges appear to move; imperfections in the camera sensor data owing to the imperfect process of recording analogue data using electronic components, including thermal noise, shot noise and interference. The accuracy obtained using this system is far in excess of that required to control ring centring.

B. Speed

During online measurements of ring geometry the system achieved a maximum frame rate of 17.2 Hz (period of 0.058 s). The processing time for each frame was 0.035 s. This frame rate does not match that of single-point measurement systems, but the density of the data makes up for that deficiency and means that this image processing system has a rate well above that required for the control of the ring rolling process described here.

V. CONCLUSION

An image processing algorithm has been presented which is capable of measuring the evolving geometry of a ring during a ring-rolling forming process. Using an off-the-shelf USB webcam and a standard desktop PC, it has been shown that a measurement frequency of 17.2 Hz can be achieved. Given the breadth of data available for the control system, this frequency is more than sufficient to control the rolling process described here.

This technique is intended to be used as the sensor in a feedback loop for the dynamic control of ring-rolling. The additional information about the geometry that it provides - high density radius data - allows the control of geometry which would be very difficult to measure and control using sensors that only record data at sparse locations around the ring.

Further improvements to this work that are planned include the estimation of angular position by tracking markers on the top surface of the ring and further speed improvements through software optimisation. A paper describing the design and implementation of a the control system is currently being prepared.

REFERENCES

- [1] "Euroforge : 2011 world-wide survey," 2011. [Online]. Available: http://www.euroforge.org/fileadmin/user_upload/Downloads/World-tons-2011_tabelle.pdf
- [2] *ASM Metals Handbook Volume 14: Forming and Forging*. ASM International, 1988.
- [3] J. M. Allwood, A. E. Tekkaya, and T. F. Stanistreet, "The development of ring rolling technology," *Steel research international*, vol. 76, no. 2-3, pp. 111–120, 2005. [Online]. Available: <http://cat.inist.fr/?aModele=afficheN&cpsidt=16530228>
- [4] B. H. Amstead, P. F. Ostwald, and M. L. Begeman, *Manufacturing processes*. Wiley, 1987. [Online]. Available: <http://books.google.co.uk/books?id=JPRTAAAMAAJ>
- [5] S. Kalpakjian and S. Schmid, *Manufacturing Engineering & Technology*. Pearson Education, 2013. [Online]. Available: http://books.google.co.uk/books?id=_ZcvAAAAQBAJ
- [6] M. R. Forouzan, M. Salimi, M. S. Gadala, and a.a. Aljawi, "Guide roll simulation in FE analysis of ring rolling," *Journal of Materials Processing Technology*, vol. 142, no. 1, pp. 213–223, Nov. 2003. [Online]. Available: <http://linkinghub.elsevier.com/retrieve/pii/S0924013603006009>
- [7] H. Meier, J. Briselat, R. Hammelmann, and H. Flick, "Image Processing Methods for Online Measurement in Radial-Axial Ring Rolling," *Proceedings of the 36th International MATADOR Conference*, 2010. [Online]. Available: http://link.springer.com/chapter/10.1007/978-1-84996-432-6_80
- [8] H. Meier, J. Briselat, T. Husmann, and D. Kreimeier, "Online Measurement of Radial-Axial Rolled Rings with an Image Processing System," *Proceedings of the 18th International Forgemasters Meeting, 2011*, 2011.
- [9] A. P. Green, "The Use of Plasticine Models to Simulate the Plastic Flow of Metals," *The philosophical magazine*, vol. 42, no. 327, pp. 365–373, 1951.
- [10] S. Y. Aku, R. A. C. Slater, and W. Johnson, "The use of plasticine to simulate the dynamic compression of prismatic blocks of hot metal," *International Journal of Mechanical ...*, vol. 9, pp. 495–525, 1967. [Online]. Available: <http://www.sciencedirect.com/science/article/pii/0020740367900513>
- [11] T. Wanheim, M. P. Schreiber, J. Gronbaek, and J. Danckert, "Physical Modelling of Metal Forming Processes," *Journal of Applied Metalworking*, vol. 1, no. 3, pp. 5–14, 1980.
- [12] M. Arentoft, Z. Gronostajski, A. Niechajowicz, and T. Wanheim, "Physical and Mathematical Modelling of Extrusion Processes," *Journal of Materials Processing Technology*, vol. 106, pp. 2–7, 2000.
- [13] T. F. Stanistreet, J. M. Allwood, and a.M. Willoughby, "The design of a flexible model ring rolling machine," *Journal of Materials Processing Technology*, vol. 177, no. 1-3, pp. 630–633, Jul. 2006. [Online]. Available: <http://linkinghub.elsevier.com/retrieve/pii/S0924013606004584>
- [14] J. M. Allwood, "A Structured Search for Novel Manufacturing Processes Leading to a Periodic Table of Ring Rolling Machines," *Journal of Mechanical Design*, vol. 129, no. 5, p. 502, 2007. [Online]. Available: <http://mechanicaldesign.asmedigitalcollection.asme.org/article.aspx?articleid=1449358>
- [15] T. Y. Kong and A. Rosenfeld, *Topological Algorithms for Digital Image Processing*, ser. Machine Intelligence and Pattern Recognition. Elsevier Science, 1996. [Online]. Available: <http://books.google.co.uk/books?id=4Yz3gKlISnwC>
- [16] R. Hartley and A. Zisserman, *Multiple view geometry in computer vision*. Cambridge university press, 2003. [Online]. Available: <http://books.google.co.uk/books?id=si3R3Pfa98QC>
- [17] J.-Y. Bouguet, "Camera calibration toolbox for matlab," 2013. [Online]. Available: http://www.vision.caltech.edu/bouguetj/calib_doc/
- [18] M. A. Oskoei and H. Hu, "A Survey on Edge Detection Methods," no. February, pp. 1–36, 2010.